

RESEARCH ARTICLE

Characterization of a nontypeable *Haemophilus influenzae* thermonuclease

Christine Cho^{1,2,3*}, Aroon T. Chande^{4,5,6*}, Lokesh Gakhar^{7,8}, Jason Hunt⁹, Margaret R. Ketterer¹⁰, Michael A. Apicella^{10*}

1 Iowa Inflammation Program, The University of Iowa, Iowa City, Iowa City, IA, United States of America, **2** Department of Infectious Disease, University of Iowa Hospitals, Iowa City, IA, United States of America, **3** Physician Scientist Training Pathway, University of Iowa Carver College of Medicine, Iowa City, IA, United States of America, **4** School of Biological Sciences, Georgia Institute of Technology, Atlanta, Georgia, United States of America, **5** IHRC-Georgia Tech Applied Bioinformatics Laboratory, Atlanta, Georgia, United States of America, **6** PanAmerican Bioinformatics Institute, Cali, Valle del Cauca, Columbia, **7** Department of Biochemistry, The University of Iowa, Iowa City, IA, United States of America, **8** Protein Crystallography Facility, The University of Iowa, Iowa City, IA, United States of America, **9** Institute for Environmental Studies, Western Illinois University, Macomb, IL, United States of America, **10** Department of Microbiology, The University of Iowa, Iowa City, IA, United States of America

* These authors contributed equally to this work.

* michael-apicella@uiowa.edu



OPEN ACCESS

Citation: Cho C, Chande AT, Gakhar L, Hunt J, Ketterer MR, Apicella MA (2018) Characterization of a nontypeable *Haemophilus influenzae* thermonuclease. PLoS ONE 13(5): e0197010. <https://doi.org/10.1371/journal.pone.0197010>

Editor: William M. Shafer, Emory University School of Medicine, UNITED STATES

Received: February 27, 2018

Accepted: April 24, 2018

Published: May 10, 2018

Copyright: © 2018 Cho et al. This is an open access article distributed under the terms of the [Creative Commons Attribution License](#), which permits unrestricted use, distribution, and reproduction in any medium, provided the original author and source are credited.

Data Availability Statement: All relevant data are within the paper.

Funding: This work was supported by the National Institute of Allergy and Infectious Diseases (<https://www.niaid.nih.gov>), grant number AI024616 to MAA; and by the Howard Hughes Medical Institute: Medical Research Fellows Program (<https://www.hhmi.org/developing-scientists/medical-research-fellows-program>), year 2009–2010 to CC. The funders had no role in study design, data collection and analysis, decision to publish, or preparation of the manuscript.

Abstract

Nontypeable *Haemophilus influenzae* (NTHi) has been shown to form biofilms, comprised of extracellular DNA (eDNA), in the middle ear and bronchus during clinical infections. Studies in our laboratory have shown that NTHi possesses a homolog of *Staphylococcus aureus* thermonuclease (staphylococcal thermonuclease), NTHi nuclease (NTHi Nuc, HI_1296). This enzyme had similar size, heat stability, and divalent cation requirements to those of the staphylococcal homolog as determined by light scattering and circular dichroism spectroscopy. Small angle X-ray scattering (SAXS) analysis suggested an overall shape and substrate-binding site comparable to those of staphylococcal nuclease. However, NTHi Nuc was approximately 25-fold more active in fluorescence resonance energy transfer (FRET) activity assay than staphylococcal thermonuclease. Homology modeling implicates shorter NTHi Nuc loops near the active site for this enhanced activity.

Introduction

Nontypeable *Haemophilus influenzae* (NTHi) are frequently found as a member of the normal upper respiratory tract bacterial flora. This species can be a frequent cause of airway infections, including otitis media in children, and sinusitis and acute exacerbations of chronic bronchitis in adults [1]. NTHi has been shown to be capable of forming biofilms *in vitro* and in the upper and lower human respiratory tract during human disease [2–4]. Bacterial biofilm matrix is an elaborate network of molecules, which can include pili, polysaccharides, double stranded extracellular DNA (eDNA), and bacterial and host derived substances that help shape and secure the biofilm to an inanimate or host surface [5]. Recent studies have shown that *Pseudomonas aeruginosa* in cystic fibrosis lung disease forms aggregates of microbes containing dead

Competing interests: The authors have declared that no competing interests exist.

and dying neutrophil, and appear to be active similar to stationary biofilms [6, 7]. The matrix protects the underlying bacteria from assault by the host immune response and antibiotic treatment thus contributing to the recalcitrant nature of biofilm to treatment [8]. An open reading frame with high homology to staphylococcal thermonuclease, called *NTHi* nuclease (*NTHi* Nuc, HI_1296), is present in the sequenced genome of *H. influenzae* strains 2019, KW20 Rd and 86-028NP. We have previously found that this nuclease is an important factor in remodeling *NTHi* biofilm [9].

In this study, we present biophysical and functional characterization of *NTHi* Nuc. FRET based enzyme kinetic studies suggested that *NTHi* Nuc was ~25 times more active than staphylococcal thermonuclease. SAXS analysis indicated that *NTHi* Nuc had a structure and DNA binding cleft similar to those of staphylococcal thermonuclease. Like the staphylococcal thermonuclease, this enzyme retained activity after heating to 65°C and required a divalent cation, magnesium or calcium, for optimal activity. This stability and increased activity of *NTHi* Nuc could play a role in efficacy of *NTHi* biofilm remodeling.

Materials and methods

Bacteria and culture conditions

Escherichia coli (*E. coli*) BL21*(DE3) was grown in Luria-Bertani (LB) medium with or without agar and supplemented with IPTG as needed.

Cloning, expression and purification of *NTHi* Nuc

NTHi Nuc without signal sequence was expressed with a cleavable 6x His-tag in pET151/D-TOPO (Life Technologies Corporations) in BL21*(DE3) *E. coli* cells and induced with 1.5 mM IPTG (Invitrogen) at 18°C. Cell cultures were pelleted and frozen at -20°C in preparation for lysis. The frozen cells were resuspended in 100 mM Tris, pH 9.1, 5 mM CaCl₂, 200 mM NaCl, 50 mM imidazole (lysis buffer) plus a mini cOmplete protease inhibitor cocktail tablet (Roche) then homogenized with an Emulsiflex 2000. His-tagged *NTHi* Nuc was bound to Ni-NTA affinity resin (Qiagen) and washed with the lysis buffer then eluted with elution buffer (lysis buffer with 250 mM imidazole). The eluted protein was concentrated and mixed with lab-purified Tobacco Etch Virus protease at 1:200 in 4°C for 16 hours to cleave the His-tag. The cleaved products were passed over a Ni Sepharose column (HisTrap FF, GE Healthcare) and the flow-through was loaded onto a gel filtration column (Superdex 75 25/60, GE Healthcare) to separate *NTHi* Nuc from contaminants and to exchange buffer into the final purification and reaction buffer: 100 mM Tris, pH 9.1, 5 mM CaCl₂, 200 mM NaCl, 5 mM DTT.

FRET assay

Nuclease enzyme activity was measured by a fluorescence resonance energy transfer activity study (FRET) assay using a Tecan Infinite M200 Pro. The FRET substrate was a single-stranded 30-mer oligonucleotide (Cy3-CCGCGAGAAACCAAGCACAGACACCGAAGA-BHQ_2) with the 5' end modified with Cy3 fluorophore and the 3' end modified with Black Hole Quencher 2 [10]. The substrate was incubated with either *NTHi* Nuc, *S. aureus* thermonuclease (Sigma-Aldrich) or RNase-free bovine pancreatic DNase I (New England Bioscience, positive control), both enzymes in DNase I reaction buffer (New England Bioscience), at 26°C, and then the absolute fluorescence was measured every 10 s for 5 min. Relative activity was calculated by,

$$\text{relative activity} = \frac{v/nM}{v_d/nM_d}$$

v is the reaction velocity of the enzyme of interest and nM is the concentration (nM) of the enzyme of interest. v_d is the reaction velocity of staphylococcal thermonuclease and nM_d is the staphylococcal thermonuclease concentration (nM). v/nM of pancreatic DNaseI was calculated based on published data [11].

Each study shown was performed a minimum of six times on multiple *NTHi* Nuc samples.

Dynamic and static light scattering

A DynaPro NanoStar instrument (Wyatt Technology, Santa Barbara) was used for all light scattering experiments and data were collected and processed with Dynamics v7 (v.7.1.7.16). Purified *NTHi* Nuc was filtered through a 0.02 µm Whatman Anotop filter and the final concentration was measured by Nanodrop 200. A 2 µl quartz cuvette was used for static light scattering (SLS), while disposable 50 µl Eppendorf UVettes (Fisher catalog # 952010051) and 4 µl plastic cuvettes (Wyatt Technology catalog # 162960 rev C) were used for dynamic light scattering (DLS). SLS measured the absolute average intensity of scattering, and DLS measured the fluctuation around the average intensity. Through multiple runs of static light scattering (SLS) and dynamic light scattering (DLS), we determined hydrodynamic radius, polydispersity, and calculated molecular weight with standard deviations.

Melting point analysis

The DynaPro NanoStar in DLS mode was used to conduct melting temperature experiments in both 50 µl and 4 µl plastic cuvettes on filtered *NTHi* Nuc samples. Rubber caps were used to seal the sample chambers during temperature ramps to minimize sample evaporation. Scattering intensity and hydrodynamic radius data were recorded as temperature was ramped at 1.0°C/min from 25°C until the protein unfolded. A sudden rapid increase of these parameters from the baseline marks the onset of protein unfolding. These T_{onset} values with standard deviations were calculated using the linear fit analysis module in Dynamics v7. Melting point data was validated with Jasco J-815 Circular Dichroism Spectropolarimeter (21-Q-1, Starna Cells Inc.) [12]. Temperature was increased by 1°C/min and spectra collected from 260–190 nm with data pitch of 1 nm, bandwidth of 1 nm, data integration time of 2 sec and scanning speed of 100 nm/min. Circular Dichroism (CD) spectrum measurements were also taken at fixed temperatures using the same parameters but with 10 measurements/spectra/temperature for higher accuracy. Purified *NTHi* Nuc was diluted to 0.5 mg/ml in phosphate buffer (PBS + 0.003% Tween-20) to reduce buffer background in CD experiments.

Homology modeling

A homology model of *NTHi* Nuc was generated using the hm_model macro in the program YASARA (YASARA Biosciences). High-resolution (1.5–1.9 Å) crystal structures of staphylococcal nuclease were used as templates and the best of five models (in terms of dihedral angles and packing scores) after simulated annealing minimization was selected as the homology model.

Small-angle X-ray scattering (SAXS)

Purified *NTHi* Nuc was dialized against SAXS buffer (100 mM Tris, pH 7 or 9, 150 mM NaCl, 5 mM CaCl, 5 mM DTT). SAXS data were collected at the SIBYLS beamline (beamline 12.3.1) at the Advanced Light Source, Lawrence Berkeley National Laboratory. The data were collected at 10°C at three concentrations in the range of 1.2–3.7 mg/ml for the sample at pH 7 and 0.4–1.2 mg/ml for the sample at pH 9. The samples were progressively exposed to

radiation for 0.5, 1, 2 and 4 seconds. Radiation damage was observed for the highest exposure for all samples and those data were not used for further analysis. Scattering data from the dialysate buffer were collected and subtracted from the protein solution scattering data. No concentration-dependent scattering was noted based on data processed from three different concentrations. Data processing was performed using the PRIMUS program package [13]. Analysis of the Guinier region (low-q region) of the scattering data for all samples at all concentrations and exposures (except the highest) was linear, suggesting that the proteins did not undergo aggregation or interparticle interference. The radius of gyration, R_g , was evaluated using the Guinier approximation at low q where $qR_g < 1.3$ [14]. The program GNOM [15] was used to compute the pair distribution function, $P(r)$, and the maximum dimension of the macromolecule, D_{max} . Experimental SAXS data were compared with simulated scattering curves in the program CRYSTAL [16] for the homology model of *NTHi Nuc* and the crystal structure of *Staphylococcal* thermonuclease (pdb id 1STN). *Ab initio* molecular envelopes were generated from the experimental scattering data using both DAMMIF [17] and GASBOR [18]. Only the highest concentration and highest exposure scattering data without radiation damage were used for *ab initio* reconstructions. Eight molecular envelopes were obtained using identical parameters but different randomly chosen values to seed the calculation. The coordinates for the models from eight runs were superimposed, averaged and filtered in the programs SUPCOMB [19] and DAMAVER [20] to create an average model, which represented the general structural features of each reconstruction, and a filtered model, which represented the core conserved features of all reconstructions. The derived molecular envelopes were visualized in PyMOL (v.1.6; Schrödinger LLC).

Statistical analysis

Statistical analysis was performed with Prism 6 software (GraphPad Software, Inc., La Jolla, CA). Values that met a p value cutoff of 0.05 were considered statistically significant.

Results

NTHi Nuc (HI_1296) is homologous to staphylococcal thermonuclease

Complete amino acid sequence of *NTHi* 2019 *Nuc* is shown in Fig 1A with the signal sequence highlighted. Fig 1B shows that *NTHi Nuc* is homologous to staphylococcal thermonuclease with 35% conserved amino acids and E-value of 2e-10.

A.						
MINRKILLTSLLILFTVLSACREKNTCRVVKISDGDTLTLCKGNKSIKVRLAEIDAPEKSQAFGQKSKTTL+						
KKTLSLDLVYQKNVRLARKGKDRTYQRTLAVVVYYQKQNINLEMVKQGMAWAYKQYSHDPTYLQAQEN						
AQAKGIGLWADNNPIEPSQWRQEKGKMAFDYQTFPSSISLFPT						
B.						
Score	Expect	Method	Identities	Positives	Gaps	
57.8 bits(138)	2e-10	Compositional matrix adjust.	47/136(35%)	75/136(55%)	21/136(15%)	
NTHi Nuc	25	KNTCRVVKISDGDTLTLCKGNKSIKVRLAEIDAPEK-----SQAFGQK-----SKTTL				74
	K+	V ++ DGDT G K IKVRL +D PE Q FG+K SKKTL+				
S. aureus	46	KDKVHVQRVVDGDTFIANQNG-KEIKVRLIGVDTPETVKPNTPVQPGKKASNYSKKTLT				104
NTHi Nuc	75	DL-VYQKNVRLARKGKDRTYQRTLAVVVYYQKQNIN-NLEMVVKQGMAWAYKQYS----HDPYI				128
	+	VY + ++ +DRY RTLA V+ K + N E+V++G+A K+S + ++				
S. aureus	105	NQDVY---LEYDEKEKQDRYGRTLAYWISKDRMYNKELVEKGGLARE-KYFSPNGKYRNVF				160
NTHi Nuc	129	IQAQENAAQAKGIGLWA 144				
		++AQ A+ + +W+				
S. aureus	161	IEAQNKAKQQQLNIWS 176				

Fig 1. Amino acid sequence of *NTHi Nuc* and its homology to staphylococcal thermonuclease. Fig 1A shows the amino acid sequence of *NTHi* 2019 *Nuc* (HI_1296). The first 20 amino acids in bold are the signal sequence of the protein. Fig 1B shows the alignment of *NTHi Nuc* with staphylococcal thermonuclease, which has 35% conserved amino acids and Expect value (number of chance matches) of 2e-10, indicating a significant match.

<https://doi.org/10.1371/journal.pone.0197010.g001>

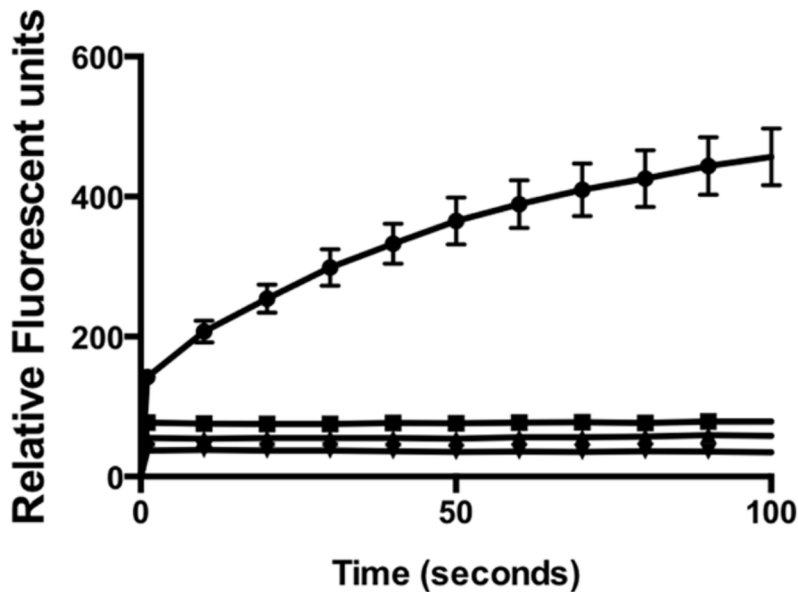


Fig 2. Effect of EDTA on *NTHi* Nuc activity. FRET assay shows single-stranded nuclease activity of *NTHi* Nuc activity. *NTHi* Nuc requires divalent cation as it lost activity with addition of EDTA. The respective lines are 0.03 nM *NTHi* Nuc alone (●), 0.03 nM *NTHi* Nuc and 0.3nM EDTA (■), 0.3nM EDTA alone (▲) and distilled water (▼). The experiment was repeated three times.

<https://doi.org/10.1371/journal.pone.0197010.g002>

Enzymatic and physicochemical characterization of *NTHi* nuclease. Enzyme activity studies were performed with PCR grade staphylococcal thermonuclease (Sigma-Aldrich) and highly purified recombinant *NTHi* Nuc without signal sequence. Signal sequence was determined by LipoP 1.0 analysis. *NTHi* Nuc possessed both single-stranded (Fig 2) and double-stranded DNA [9] nuclease activity. *NTHi* Nuc was a highly efficient nuclease with greater than 1500 fold increased activity compared to bovine pancreatic DNase I and greater than 25 fold increased activity compared to staphylococcal thermonuclease (Table 1). *NTHi* Nuc activity was greatest near pH 9, similar to staphylococcal thermonuclease, however *NTHi* Nuc retained some activity over a range of pH 5–9.5 (data not shown). *NTHi* Nuc activity was also temperature dependent with maximum at 37°C. Of note, *NTHi* Nuc remained active at 4°C and 25°C for several months in sterile solution and retained endo-exonuclease activity above 45°C in pH = 8.5; heating to 60°C partially denatured the protein. Heat-denatured *NTHi* Nuc, when cooled to 25°C, re-established its activity and was able to degrade DNA (Fig 3). *NTHi* Nuc and staphylococcal thermonucleases are most active near their pIs [21], similarly both staphylococcal thermonuclease and *NTHi* Nuc are competitively inhibited by thymidine

Table 1. FRET assay of *NTHi* Nuc activity.

Sample	Concentration nM	Velocity/nM	Relative activity compared to staphylococcal thermonuclease
<i>NTHi</i> Nuc	0.035	158.4	23
<i>NTHi</i> Nuc + 0.015 nM pdTp	0.035	26.3	4
<i>NTHi</i> Nuc + 0.03 nM pdTp	0.035	20.3	3
Staphylococcal thermonuclease	0.278	6.8	1
Bovine pancreatic DNase I	6	0.1*	0.015

* calculated based on published data [11]

<https://doi.org/10.1371/journal.pone.0197010.t001>

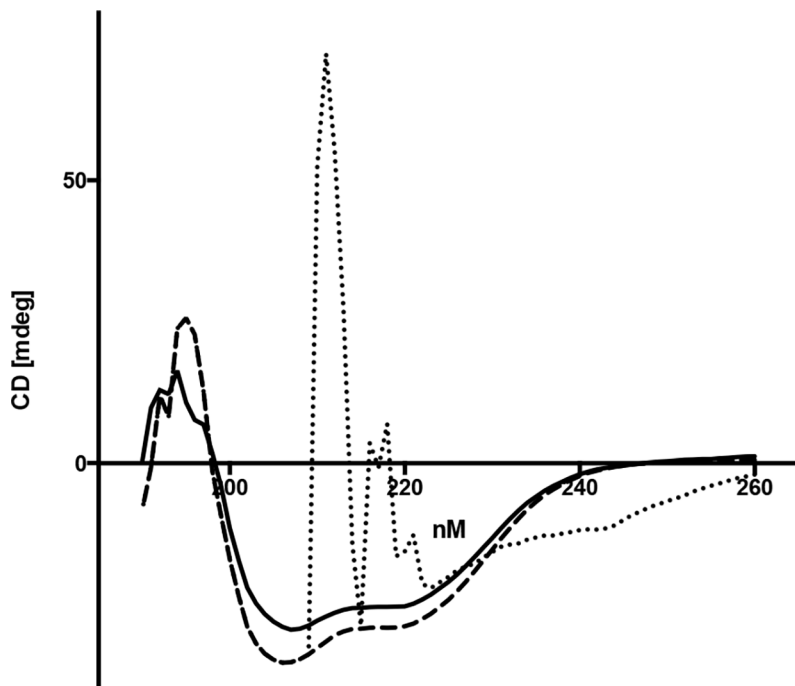


Fig 3. CD spectra of *NTHi* Nuc from 190–260 nm. This figure shows representative curves. When *NTHi* Nuc was heated from 25°C (solid line) to 60°C (dotted line), the spectra was lost, indicating loss of secondary structure. When the sample was then cooled to 25°C (dashed line), *NTHi* Nuc underwent reversible thermal folding. Samples were referenced to buffer.

<https://doi.org/10.1371/journal.pone.0197010.g003>

3,5-bisphosphate (pdTp), a DNA mimic [22]. Half and equimolar concentrations of pdTp impacted initial rates of endonuclease activity (Table 1). However, at low substrate concentration at 300 seconds, half-molar nuclease-pdTp reactions had approximately twice the activity of equimolar nuclease-pdTp reactions (Fig 4).

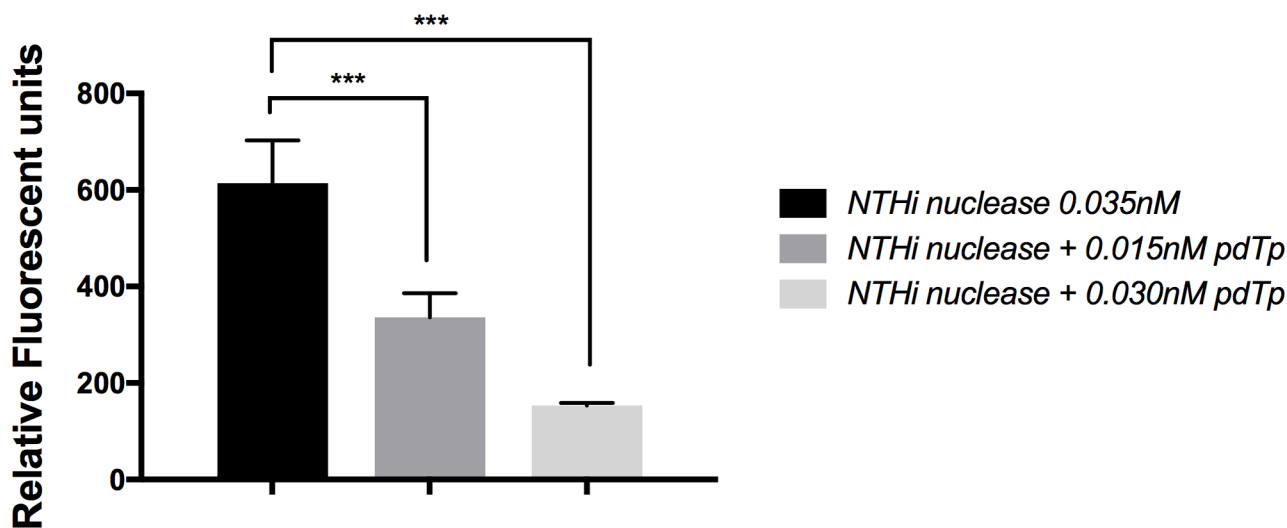


Fig 4. Effect of inhibitor on *NTHi* Nuc activity. *NTHi* Nuc was incubated with 2 μM FRET substrate and increasing concentrations of inhibitor (pdTp). Enzyme activity was measured in FRET assay. $n = 3$ for 0.03nM of pdTp and $n = 2$ for 0.015nM of pdTp. Relative fluorescent units decreased as pdTp concentration increased, thus indicating that the inhibitor acts as a competitive inhibitor for *NTHi* Nuc when low concentration of the substrate was present, as measured by FRET. Bars represent the average from three independent experiments for 0.03nM of pdTp and two independent experiments for 0.015nM of pdTp ± SD. p-values were determined using two-sided student's t test with assumption of equal variance (** p-value < 0.0005).

<https://doi.org/10.1371/journal.pone.0197010.g004>

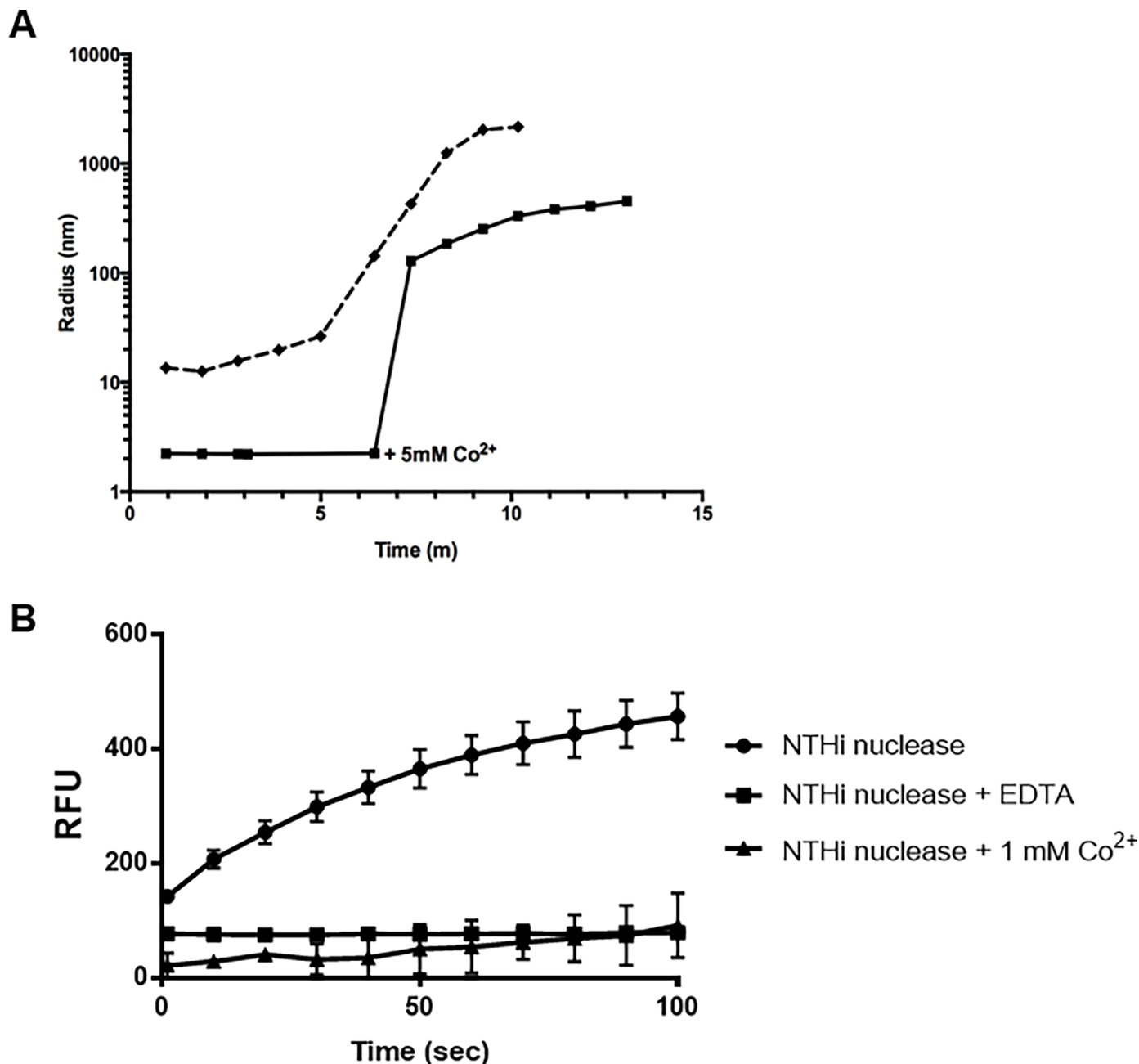


Fig 5. Effect of Co²⁺ on NTHi Nuc structure and activity. NTHi Nuc with Ca²⁺ has a hydrodynamic radius of approximately 2.1 nm when in solution. Within minutes of adding Co²⁺, a known inhibitor for staphylococcal thermonuclease, the size of NTHi Nuc increased dramatically indicating oligomerization or nonspecific aggregation (solid line in Panel A). The aggregates formed by the addition of Co²⁺ to NTHi Nuc were briefly disrupted by passing the solution through a 0.22 μm membrane filter reduced the hydrodynamic radius to approximately 15 nm (start of dashed line in Panel A). However, NTHi Nuc continued aggregating and increasing in size due to Co²⁺ still present in solution (dashed line). Panel A shows representative curves. Activity of NTHi Nuc was quenched with addition of Co²⁺ when measured by FRET, similar to when EDTA was added (Panel B). Panel A shows representative curves and Panel B was done in triplicates.

<https://doi.org/10.1371/journal.pone.0197010.g005>

Divalent cation dependence

EDTA chelation quenched NTHi Nuc activity (Fig 2), highlighting divalent cation requirement for its activity. Addition of Ca²⁺ or Mg²⁺ restored NTHi Nuc activity (data not shown). Either Ca²⁺ or Mg²⁺ was required, but not both, as NTHi Nuc activity was unchanged when

Table 2. Light Scattering demonstrating effect of pH on NTH*i* Nuc size.

pH	Radius (nm)	Polydispersity (%)	SLS MW (kDa)
7	2.19 ± 0.04	13.1 ± 0.3	19.3 ± 0.0
8	2.64 ± 0.04	32.5 ± 1.8	—
9	2.53 ± 0.01	20.3 ± 1.1	—

<https://doi.org/10.1371/journal.pone.0197010.t002>

Table 3. Effect of pH on thermal stability.

	T _{onset}
NTH <i>i</i> Nuc pH 7	40.2 ± 0.5
NTH <i>i</i> Nuc pH 7 + pdTp (excess)	48.1 ± 1.45
NTH <i>i</i> Nuc pH 8	45.1 ± 0.1
NTH <i>i</i> Nuc pH 9	53.2 ± 0.1
Staphylococcal thermonuclease pH 7 ¹	45.8
Staphylococcal thermonuclease pH 8 ²	46

¹ –Calculated from published data [24, 25]

² –Calculated from published data (38)

<https://doi.org/10.1371/journal.pone.0197010.t003>

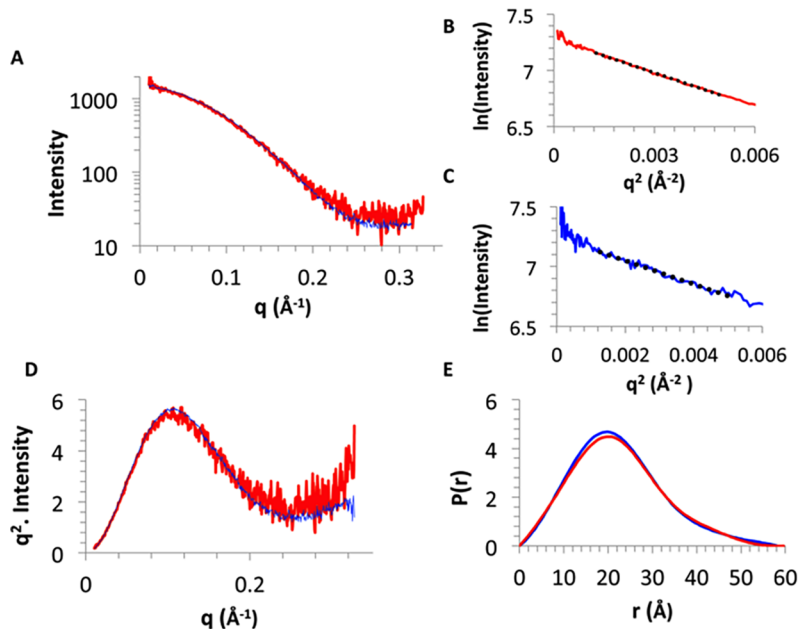


Fig 6. SAXS analysis of NTH*i* Nuc. Fig 6A shows scaled SAXS scattering curves of NTH*i* Nuc in pH = 7 (blue) and 9 (red). There were no gross structural changes at those two pH. Fig 6B and Fig 6C show Guinier plot for NTH*i* Nuc at pH = 7 and 9, respectively. Rg was 17.4 Å at both pH. Fig 6D shows parabolic Kratky plots in pH 7 (blue) and 9 (red), showing some flexible region. Fig 6E shows pairwise distribution function plots at pH 7 (blue) and 9 (red), with maximum dimensions of 58.3 Å at pH 7 and 59.6 Å at pH 9.

<https://doi.org/10.1371/journal.pone.0197010.g006>

both Ca²⁺ or Mg²⁺ were added (data not shown). Cobalt, an inhibitor of staphylococcal thermonuclease [23], not only aggregated NTH*i* Nuc structure (Fig 5. Panel A), but also quenched its activity, similar to addition of EDTA (Fig 5. Panel B).

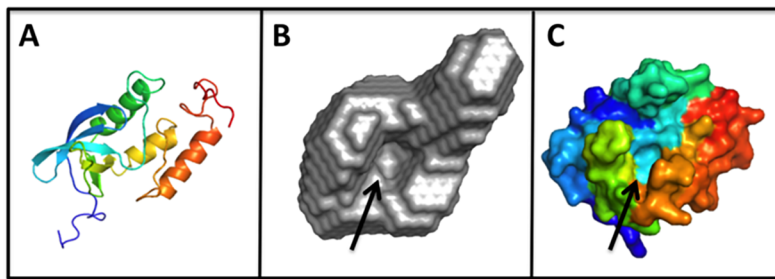


Fig 7. Structure of NTHi Nuc by SAXS. Fig 7A shows a homology model of NTHi Nuc shown as a cartoon, blue = N-terminal and red = C-terminal. Fig 7B shows the *ab initio* shape of NTHi Nuc determined from SAXS data at pH 7. Fig 7C shows the surface representation of staphylococcal thermonuclease crystal structure. Fig 7B and 7C show similar overall shape and active site (black arrow).

<https://doi.org/10.1371/journal.pone.0197010.g007>

Static and dynamic light scattering

Static and Dynamic Light Scattering (SLS/DLS) were used to determine the biophysical characteristics of NTHi nuclease. Molecular weight determination from SLS shows no oligomerization at pH 7 (Table 2). At pH 9, hydrodynamic radius increased, indicating a larger open conformation (Table 2). Protein stability at various pH was reported as melting temperatures, T_{onset} , in Table 3. NTHi Nuc was most stable around pH 9 with a reported T_{onset} of 53 °C. Comparatively, the T_{onset} of staphylococcal thermonuclease is 45.8 °C at pH 7 (calculated from published data; [24]). At pH 7, excess pdTp increased NTHi Nuc thermal stability, reported as a T_{onset} from 40 °C to 48 °C (Table 3). In addition to pH dependence, NaCl and divalent cations were assayed for effects on stability of NTHi Nuc. DLS showed that NTHi Nuc was stable between 50 mM and 1M of NaCl, below and above physiological concentrations (data not shown). When Ca^{2+} was replaced with Co^{2+} , NTHi Nuc aggregated (Fig 5. Panel A) and activity was lost (Fig 5. Panel B). Passing NTHi Nuc + Co^{2+} through a 0.22 μm membrane filter removed these aggregates and re-aggregation can be quantified in real time using DLS (Fig 5. Panel A).

Small-angle X-ray scattering

The Guinier analysis resulted in R_g values of 17.4 Å at both pH 7 and pH 9. The radius of gyration of the homology model as calculated by CRYSTAL was 17.0 Å indicating that NTHi Nuc was a monomer in solution. Pairwise distance distribution function, $P(r)$, showed maximum dimension, D_{max} , of 58.3 and 59.6 Å (Fig 6) at pH 7 and 9, respectively. These data indicate that despite the significant difference in activity of NTHi Nuc at pH 7 and 9, there were no global conformation changes. The *ab initio* model had features, such as the active site cavity, that were remarkably similar to that of staphylococcal nuclelease (Fig 7) indicating similarity between NTHi nuclease and staphylococcal thermonuclease. However, the three loops, including the Ω loop near the calcium ion, forming the metal binding and active site in NTHi Nuc homology model were predicted to be shorter than the corresponding loops in staphylococcal nuclease (Fig 8).

Discussion

A number of bacterial species responsible for causing human disease including *Staphylococcus aureus*, *Neisseria gonorrhoeae*, *Streptococcus sanguinis*, *Serratia marscens*, *Campylobacter jejuni*, *Enterococcus faecalis* and *Bacillus anthracis* encode a thermonuclease. The functional properties and structure of the *S. aureus* thermonuclease has been studied for almost 50 years [26].

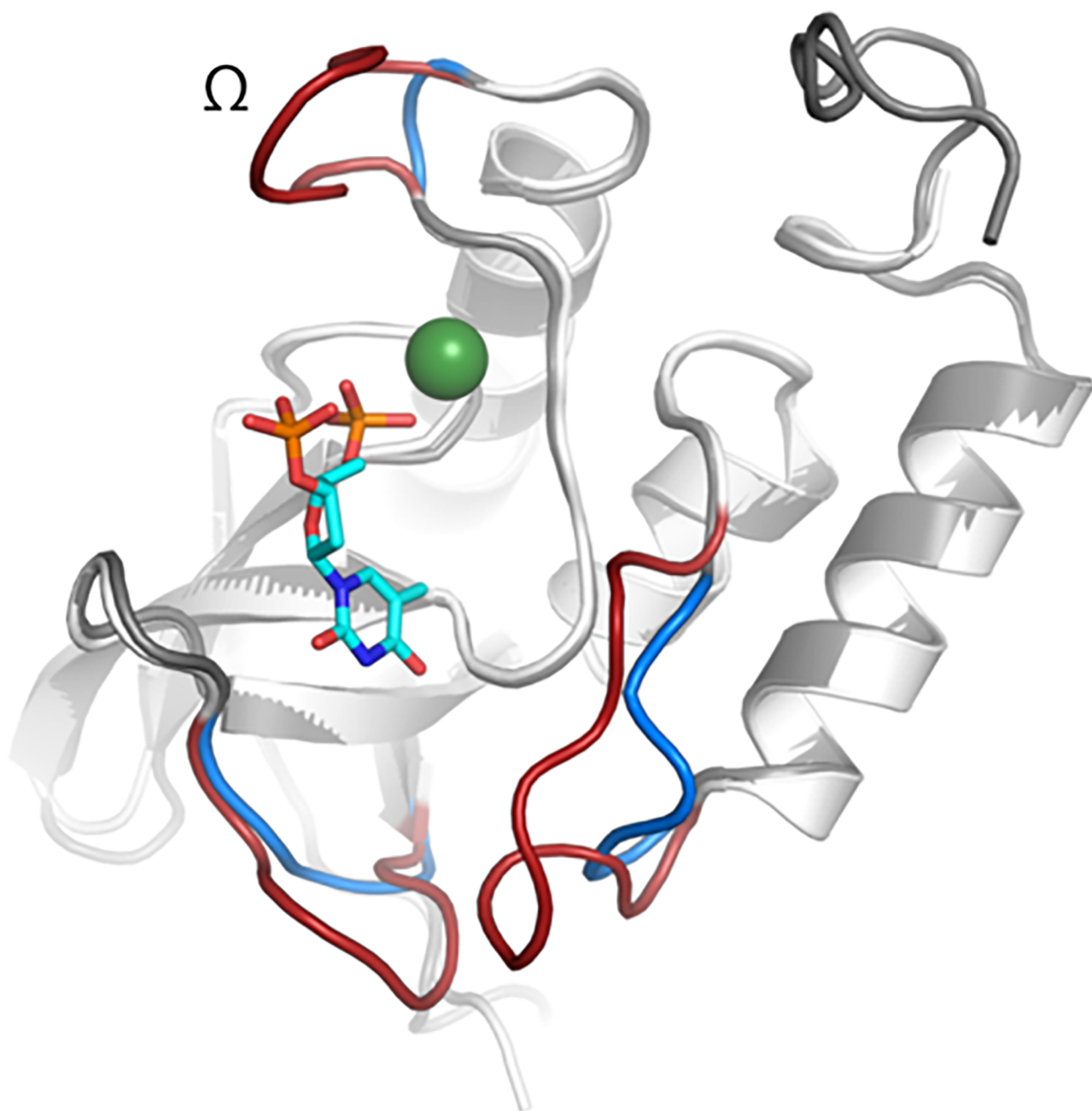


Fig 8. Homology model comparison of *NTHi* Nuc to staphylococcal thermonuclease. Overlay of the homology model of *NTHi* Nuc (blue), and the active site of staphylococcal thermonuclease (pdb id 1STN) (red). Green sphere represents calcium and cyan sticks represent TdtP (inhibitor); modeled from pdb id 2SNS. There are three loops in the active site of *NTHi* Nuc that are shorter than those of staphylococcal thermonuclease. The absence of Ω loop near the active site of *NTHi* Nuc compared to the staphylococcal thermonuclease could contribute to the stronger activity of *NTHi* Nuc.

<https://doi.org/10.1371/journal.pone.0197010.g008>

Studies have shown that *S. aureus* and *N. gonorrhoeae* encode nucleases, which play a role in remodeling the extracellular DNA (eDNA) matrix of the biofilm formed by the respective organisms [27, 28]. In addition, it has been shown that the nucleases of *N. gonorrhoeae*, *S. aureus* and *S. sanguinis* protect the microbes from neutrophil extracellular trap-mediated bactericidal activity [29–31]. Our previous study evaluated the role of *NTHi* Nuc in biofilm by *NTHi* [9]. This study further characterizes the *NTHi* enzyme in detail. *NTHi* Nuc has 35%

identity and 55% similarity to staphylococcal thermonuclease. Similar to the staphylococcal thermonuclease, *NTHi* Nuc could be inactivated by heating to 65 °C, but could refold to its active form at 25°C. Unlike staphylococcal nuclease, which has no cysteines, *NTHi* Nuc has three cysteines, two of which were predicted to be on neighboring beta strands in the homology model, capable of forming a disulfide bond that could potentially contribute to its high thermostability. *NTHi* Nuc was approximately 25 and 1500 times more potent than staphylococcal thermonuclease and DNase I, respectively. Low resolution SAXS analysis indicated that *NTHi* Nuc had a similar binding pocket and general shape as staphylococcal thermonuclease, but predicted to have shorter loops forming the metal binding and active sites compared to those of staphylococcal thermonuclease, including the Ω loop. Previous studies have shown that the deletion of staphylococcal thermonuclease Ω loop had increased stability compared to the staphylococcal thermonuclease with an active site mutation [32, 33]. Therefore, the absence of the Ω loop in *NTHi* Nuc could play a role in the enhanced activity of the *NTHi* Nuc. The other two shorter loops in *NTHi* Nuc active site could also allow space for larger substrates, which may also contribute to the enhanced activity of the *NTHi* Nuc. The melting temperatures and optimal pH for enzymatic activity are similar for both enzymes. *NTHi* Nuc required divalent cations, Mg²⁺ or Ca²⁺, for its activity. *NTHi* Nuc can digest both double- and single-stranded eDNA.

Our previous work has shown that *NTHi nuc* expression is crucial for biofilm remodeling and dispersal. We were surprised that while the nuclease was regulated, there was only 1.52-fold increased gene expression in planktonic phase compared to those of biofilm phase. The high potency of *NTHi* Nuc suggests that this tight regulation of expression was necessary to disperse organisms from biofilm and was required to maintain biofilm homeostasis.

The use of exogenous nucleases has been suggested to treat chronic biofilm infections in the respiratory tract in illnesses such as cystic fibrosis [34, 35]. Given the potency of the *NTHi* nuclease, it may find a role in management of such disease processes. In addition, the *NTHi* nuclease could find usefulness in industrial processes such as production of flavor enhancers [36] and in treatment of food processing equipment contaminated with DNA containing biofilms [37].

Acknowledgments

This work was supported by NIAID grant AI024616 (MAA). CC was supported to perform this work by a Howard Hughes Medical Student Fellowship. This research used resources of the Advanced Light Source (ALS), which is a DOE Office of Science User Facility operated by the Lawrence Berkeley National Laboratory under contract no. DE-AC02-05CH11231. We thank the staff at the SIBYLS 12.3.1 ALS beamline supported through the Integrated Diffraction Analysis Technologies program (DOE Office of Biological and Environmental Research) and the National Institute of Health project MINOS (R01GM105404) for SAXS data collection.

Author Contributions

Conceptualization: Christine Cho, Michael A. Apicella.

Data curation: Christine Cho, Aroon T. Chande, Lokesh Gakhar, Jason Hunt, Margaret R. Ketterer, Michael A. Apicella.

Formal analysis: Christine Cho, Lokesh Gakhar.

Funding acquisition: Michael A. Apicella.

Methodology: Christine Cho, Aroon T. Chande, Jason Hunt, Margaret R. Ketterer, Michael A. Apicella.

Project administration: Michael A. Apicella.

Resources: Michael A. Apicella.

Software: Lokesh Gakhar.

Supervision: Michael A. Apicella.

Writing – original draft: Aroon T. Chande, Michael A. Apicella.

Writing – review & editing: Christine Cho, Aroon T. Chande, Lokesh Gakhar, Jason Hunt, Michael A. Apicella.

References

1. Murphy TF, Apicella MA. Nontypable *Haemophilus influenzae*: a review of clinical aspects, surface antigens and the human response to infection. *Rev Infect Dis.* 1987; 9:1–15. PMID: [3547567](#)
2. Chin CL, Manzel LJ, Lehman EE, Humlincek AL, Shi L, Starner TD, et al. Haemophilus influenzae from patients with chronic obstructive pulmonary disease exacerbation induce more inflammation than colonizers. *Am J Respir Crit Care Med.* 2005; 172(1):85–91. Epub 2005/04/05. <https://doi.org/10.1164/rccm.200412-1687OC> PMID: [15805181](#); PubMed Central PMCID: [PMC2718449](#).
3. Post JC. Direct evidence of bacterial biofilms in otitis media. *Laryngoscope.* 2001; 111(12):2083–94. <https://doi.org/10.1097/00005537-200112000-00001> PMID: [11802002](#).
4. Starner TD, Zhang N, Kim G, Apicella MA, McCray PB Jr. *Haemophilus influenzae* forms biofilms on airway epithelia: implications in cystic fibrosis. *Am J Respir Crit Care Med.* 2006; 174(2):213–20. Epub 2006/05/06. <https://doi.org/10.1164/rccm.200509-1459OC> PMID: [16675778](#); PubMed Central PMCID: [PMC2662906](#).
5. Stoodley P, Sauer K, Davies DG, Costerton JW. Biofilms as complex differentiated communities. *Annu Rev Microbiol.* 2002; 56:187–209. <https://doi.org/10.1146/annurev.micro.56.012302.160705> PMID: [12142477](#).
6. Caceres SM, Malcolm KC, Taylor-Cousar JL, Nichols DP, Saavedra MT, Bratton DL, et al. Enhanced in vitro formation and antibiotic resistance of nonattached *Pseudomonas aeruginosa* aggregates through incorporation of neutrophil products. *Antimicrob Agents Chemother.* 2014; 58(11):6851–60. Epub 2014/09/04. <https://doi.org/10.1128/AAC.03514-14> PMID: [25182651](#); PubMed Central PMCID: [PMCPMC4249413](#).
7. Maunders E, Welch M. Matrix exopolysaccharides; the sticky side of biofilm formation. *FEMS Microbiol Lett.* 2017; 364(13). Epub 2017/06/13. <https://doi.org/10.1093/femsle/fnx120> PMID: [28605431](#); PubMed Central PMCID: [PMCPMC5812517](#).
8. Mah TF, O'Toole GA. Mechanisms of biofilm resistance to antimicrobial agents. *Trends Microbiol.* 2001; 9(1):34–9. Epub 2001/02/13. PMID: [11166241](#).
9. Cho C, Chande A, Gakhar L, Bakalatz LO, Jurcisek JA, Ketterer M, et al. Role of the nuclease of non-typeable *Haemophilus influenzae* in dispersal of organisms from biofilms. *Infect Immun.* 2015; 83(3):950–7. Epub 2014/12/31. <https://doi.org/10.1128/IAI.02601-14> PMID: [25547799](#); PubMed Central PMCID: [PMCPMC4333478](#).
10. Lee SP, Porter D, Chirikjian JG, Knutson JR, Han MK. A fluorometric assay for DNA cleavage reactions characterized with BamHI restriction endonuclease. *Anal Biochem.* 1994; 220(2):377–83. Epub 1994/08/01. <https://doi.org/10.1006/abio.1994.1353> PMID: [7978282](#).
11. Zhou Z, Zhu C, Ren J, Dong S. A graphene-based real-time fluorescent assay of deoxyribonuclease I activity and inhibition. *Analytica chimica acta.* 2012; 740:88–92. Epub 2012/07/31. <https://doi.org/10.1016/j.aca.2012.06.032> PMID: [22840655](#).
12. Greenfield NJ. Using circular dichroism spectra to estimate protein secondary structure. *Nature protocols.* 2006; 1(6):2876–90. <https://doi.org/10.1038/nprot.2006.202> PMID: [17406547](#); PubMed Central PMCID: [PMC2728378](#).
13. Konarev P. PRIMUS: a Windows PC-based system for small-angle scattering data analysis. *Journal of Applied Crystallography* 2003; 36:1277–82.
14. Guinier A, Fournet G, Yudowitch KL. Small-angle scattering of X-rays. New York, NY: Wiley; 1955.

15. Semenyuk A, Svergun DI. GNOM-a program package for small-angle scattering data processing. *Journal of Applied Crystallography* 1991; 24:5:537–40.
16. Svergun D, Barberato C, Koch MHJ. CRYSTOL-a program to evaluate X-ray solution scattering of biological macromolecules from atomic coordinates. *Journal of Applied Crystallography* 1995; 28:6:768–73.
17. Svergun DI. Restoring low resolution structure of biological macromolecules from solution scattering using simulated annealing. *Biophysical journal*. 1999; 76(6):2879–86. Epub 1999/06/04. [https://doi.org/10.1016/S0006-3495\(99\)77443-6](https://doi.org/10.1016/S0006-3495(99)77443-6) PMID: 10354416; PubMed Central PMCID: PMC1300260.
18. Svergun DI, Petoukhov MV, Koch MH. Determination of domain structure of proteins from X-ray solution scattering. *Biophysical journal*. 2001; 80(6):2946–53. Epub 2001/05/24. [https://doi.org/10.1016/S0006-3495\(01\)76260-1](https://doi.org/10.1016/S0006-3495(01)76260-1) PMID: 11371467; PubMed Central PMCID: PMC1301478.
19. Kozin MB, Svergun DI. Automated matching of high-and low-resolution structural models. *Journal of Applied Crystallography* 2001; 34:1.
20. Volkov V, Svergun D. Uniqueness of ab initio shape determination in small-angle scattering. *Journal of Applied Crystallography*. 2003; 36:3:860–4.
21. Trucks DM, Somoza JR, Prehoda KE, Miller SC, Markley JL. Coupling between trans/cis proline isomerization and protein stability in staphylococcal nuclease. *Protein Sci.* 1996; 5(9):1907–16. Epub 1996/09/01. <https://doi.org/10.1002/pro.5560050917> PMID: 8880915; PubMed Central PMCID: PMC2143535.
22. Tucker PW, Hazen EE Jr., Cotton FA. Staphylococcal nuclease reviewed: a prototypic study in contemporary enzymology. II. Solution studies of the nucleotide binding site and the effects of nucleotide binding. *Mol Cell Biochem*. 1979; 23(1):3–16. Epub 1979/01/15. PMID: 423893.
23. Loll PJ, Quirk S, Lattman EE, Garavito RM. X-ray crystal structures of staphylococcal nuclease complexed with the competitive inhibitor cobalt(II) and nucleotide. *Biochemistry*. 1995; 34(13):4316–24. Epub 1995/04/04. PMID: 7703245.
24. Su Z, Wu JM, Fang HJ, Tsong TY, Chen HM. Local stability identification and the role of a key aromatic amino acid residue in staphylococcal nuclease refolding. *Febs J*. 2005; 272(15):3960–6. Epub 2005/07/28. <https://doi.org/10.1111/j.1742-4658.2005.04814.x> PMID: 16045766.
25. Calderon RO, Stolowich NJ, Gerlt JA, Sturtevant JM. Thermal denaturation of staphylococcal nuclease. *Biochemistry*. 1985; 24(22):6044–9. Epub 1985/10/22. PMID: 3910087.
26. Cunningham L. Micrococcal nuclease and some products of its action. *Ann N Y Acad Sci*. 1958; 3(1):27–39.
27. Steichen CT, Cho C, Hunt J, Shao J, Apicella MA. The Neisseria gonorrhoeae Biofilm Matrix Contains DNA and an Endogenous Nuclease Controls its Incorporation. *Infection and Immunity*. 2011; Epub (February 7).
28. Olson ME, Nygaard TK, Ackermann L, Watkins RL, Zurek OW, Pallister KB, et al. Staphylococcus aureus nuclease is an SaeRS-dependent virulence factor. *Infection and Immunity*. 2013; 81(4):1316–24. Epub 2013/02/06. <https://doi.org/10.1128/IAI.01242-12> PMID: 23381999; PubMed Central PMCID: PMC3639593.
29. Morita C, Sumioka R, Nakata M, Okahashi N, Wada S, Yamashiro T, et al. Cell wall-anchored nuclease of Streptococcus sanguinis contributes to escape from neutrophil extracellular trap-mediated bactericidal activity. *PLoS One*. 2014; 9(8):e103125. <https://doi.org/10.1371/journal.pone.0103125> PMID: 25084357; PubMed Central PMCID: PMC4118848.
30. Juneau RA, Stevens JS, Apicella MA, Criss AK. A thermonuclease of Neisseria gonorrhoeae enhances bacterial escape from killing by neutrophil extracellular traps. *J Infect Dis*. 2015; 212(2):316–24. <https://doi.org/10.1093/infdis/jiv031> PMID: 25605868; PubMed Central PMCID: PMC4490236.
31. Thammavongsa V, Missiakas DM, Schneewind O. Staphylococcus aureus degrades neutrophil extracellular traps to promote immune cell death. *Science*. 2013; 342(6160):863–6. <https://doi.org/10.1126/science.1242255> PMID: 24233725; PubMed Central PMCID: PMC4026193.
32. Poole LB, Loveys DA, Hale SP, Gerlt JA, Stanczyk SM, Bolton PH. Deletion of the omega-loop in the active site of staphylococcal nuclease. 1. Effect on catalysis and stability. *Biochemistry*. 1991; 30(15):3621–7. Epub 1991/04/16. PMID: 2015219.
33. Baldissari DM, Torchia DA, Poole LB, Gerlt JA. Deletion of the omega-loop in the active site of staphylococcal nuclease. 2. Effects on protein structure and dynamics. *Biochemistry*. 1991; 30(15):3628–33. Epub 1991/04/16. PMID: 2015220.
34. Whitchurch CB, Tolker-Nielsen T, Ragas PC, Mattick JS. Extracellular DNA required for bacterial biofilm formation. *Science*. 2002; 295(5559):1487. <https://doi.org/10.1126/science.295.5559.1487> PMID: 11859186.
35. Cavaliere R, Ball JL, Turnbull L, Whitchurch CB. The biofilm matrix destabilizers, EDTA and DNaseI, enhance the susceptibility of nontypeable *Hemophilus influenzae* biofilms to treatment with ampicillin

- and ciprofloxacin. *Microbiologyopen*. 2014; 3(4):557–67. <https://doi.org/10.1002/mbo3.187> PMID: 25044339; PubMed Central PMCID: PMC4287182.
36. Cairoli P, Pieraccini S, Sironi M, Morelli CF, Speranza G, Manitto P. Studies on umami taste. Synthesis of new guanosine 5'-phosphate derivatives and their synergistic effect with monosodium glutamate. *J Agric Food Chem*. 2008; 56(3):1043–50. <https://doi.org/10.1021/jf072803c> PMID: 18181569.
37. Zetzmann M, Sanchez-Kopper A, Waidmann MS, Blombach B, Riedel CU. Identification of the agr Peptide of *Listeria monocytogenes*. *Front Microbiol*. 2016; 7:989. <https://doi.org/10.3389/fmicb.2016.00989> PMID: 27446029; PubMed Central PMCID: PMC4916163.